IAA-PDC13-04-27
Catching a Rolling Stone: Dynamics and Control of a Spacecraft and an Asteroid

Carlos M. Roithmayr*

NASA Langley Research Center, Vehicle Analysis Branch
MS 451, 1 North Dryden Street, Hampton, VA, 23681, USA +1 757 864 6778
carlos.m.roithmayr@nasa.gov

Haijun Shen, Mark Jesick, and David M. Cornelius

Analytical Mechanics Associates, Inc.
303 Butler Farm Rd., Suite 104A, Hampton, VA 23666, USA +1 757 865 0000
shen@ama-inc.com, mark.c.jesick@ama-inc.com, cornelius@ama-inc.com

Abstract

In a recent report, a robotic spacecraft mission is proposed for the purpose of collecting a small asteroid, or a small part of a large one, and transporting it to an orbit in the Earth-Moon system. Such an undertaking will require solutions to many of the engineering problems associated with deflection of an asteroid that poses a danger to Earth. In both cases, it may be necessary for a spacecraft to approach an asteroid from a nearby position, hover for some amount of time, move with the same angular velocity as the asteroid, descend, perhaps ascend, and finally arrest the angular velocity of the asteroid. Dynamics and control in each of these activities is analyzed in order to determine the velocity increments and control torque that must be provided by a reaction control system, and the mass of the propellant that will be consumed. Two attitude control algorithms are developed, one to deal with synchronizing the spacecraft's angular velocity with that of the asteroid, and the other to arrest the asteroid's angular velocity. A novel approach is proposed for saving fuel in the latter case.

Keywords: asteroid capture, rotational motion, rendezvous, trajectory control, attitude control

1. Introduction

The National Aeronautics and Space Administration (NASA) is currently investigating a conceptual robotic mission to collect a small Near-Earth Asteroid (NEA) or a small boulder resting on the surface of a large NEA, and transport it to an orbit in the Earth-Moon system. An object with a diameter of roughly 7 m is of interest. Such a mission would lead to greater scientific understanding of NEAs and serve as preparation for planetary defense. This paper is concerned with dynamics and control of the spacecraft trajectory and attitude in the terminal phases of a rendezvous with the object, as well as the attitude of the spacecraft after its payload has been secured.

The objective of NASA's investigation is to consider in further detail the mission proposed in Ref. [1]. Figure 1 illustrates aspects of the mission that are especially relevant to a study of dynamics and control. An asteroid, A, is to be collected by a spacecraft, B, using a container that is essentially axisymmetric. In Fig. 1, $\hat{\mathbf{b}}_3$ is a unit vector fixed in B and parallel to the container's axis of symmetry. A few assumptions that strongly influence the direction of study can be made based on the configuration of the container. First of all, placement of the container's opening requires B to advance in the direction of $\hat{\mathbf{b}}_3$ as it collects

*Corresponding author

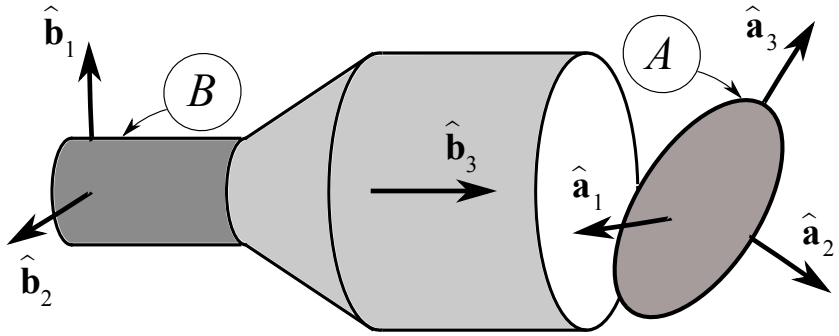

Figure 1: Asteroid, A, Collected by Spacecraft, B, with Axisymmetric Container

A. Secondly, as long as the diameter of the container exceeds the largest dimension of A, collection can be accomplished without restricting the relative orientation about $\hat{\mathbf{b}}_3$ between A and B. We assume that in order to prevent damage to the container, two requirements must be imposed: as B approaches A, $\hat{\mathbf{b}}_3$ must remain collinear with a line fixed in A, and there must be no relative angular velocity between A and B when the two make contact. Finally, we assume that the angular velocity of B relative to an inertial reference frame must be made to vanish after A is collected. This is necessary, for example, to orient solar arrays properly or to aim thrust in the direction needed to return to the Earth-Moon system.

Small asteroids, which are more numerous than large ones and collide with Earth more frequently, could with sufficient warning time be deflected by using such a spacecraft. The spacecraft could also be used to collect a small asteroid for the purpose of deflecting a large one, as proposed in Ref. [2].

Throughout what follows, the spacecraft B is regarded as a rigid body. As discussed in Ref. [1], the mass of B is 18,000 kg. The bus (without the container) is axisymmetric, with a diameter of 2.7 m and a height of 5.9 m. For the purpose of this study, we presume the container is light in comparison to the bus, and mass is distributed uniformly in the cylindrical bus. In that case I_r, central principal moments of inertia of B (that is, principal moments of inertia relative to the mass center of B) for unit vectors $\hat{\mathbf{b}}_r$ $(r = 1, 2, 3)$, are determined to be $I_1 = I_2 = 60416$ kg-m^2, and $I_3 = 16403$ kg-m^2. Four pods, each containing four Reaction Control System (RCS) thrusters, are mounted to the bus on struts as shown in Fig. 5 of Ref. [1] (p. 23). Each pod has a radial distance of 2 m from the cylinder's axis of symmetry, and is 0.3 m from the cylinder's end. Each thruster can apply 200 N of force, and has a specific impulse $I_{\text{sp}} = 287$ s. The position vector $\mathbf{r}^{B^\star P_r}$ from the mass center of the bus, $B^\star$, to each of the four pods P_r $(r = 1, 2, 3, 4)$, and directions of thrust, are reported in Table 1.

Table 1: RCS Thruster Configuration

Pod	Position (m)	Thrust Directions
P_1	$\mathbf{r}^{B^\star P_1} = \quad 2\hat{\mathbf{b}}_1 - 2.65\hat{\mathbf{b}}_3$	$\pm\hat{\mathbf{b}}_2, \pm\hat{\mathbf{b}}_3$
P_2	$\mathbf{r}^{B^\star P_2} = -2\hat{\mathbf{b}}_1 - 2.65\hat{\mathbf{b}}_3$	$\pm\hat{\mathbf{b}}_2, \pm\hat{\mathbf{b}}_3$
P_3	$\mathbf{r}^{B^\star P_3} = \quad 2\hat{\mathbf{b}}_2 - 2.65\hat{\mathbf{b}}_3$	$\pm\hat{\mathbf{b}}_1, \pm\hat{\mathbf{b}}_3$
P_4	$\mathbf{r}^{B^\star P_4} = -2\hat{\mathbf{b}}_2 - 2.65\hat{\mathbf{b}}_3$	$\pm\hat{\mathbf{b}}_1, \pm\hat{\mathbf{b}}_3$

Whereas the foregoing description of B can be given quantitatively, a corresponding concrete description of A is not available because the particular object to be collected has not yet been identified. Moreover, there is a paucity of accurate information about 10-m asteroids, and such information is not easily obtained. Consequently, to make progress in analysis we must fabricate our own asteroids and assign each of them a heliocentric orbit, physical dimensions, mass, distribution of mass, and rotational motion. In practice, it

will be important to design the spacecraft to be able to deal with a healthy amount of uncertainty in these and other asteroid parameters.

We consider the process of collecting A to consist of the following steps. B leads or trails A in its orbit at a nearby position that is stationary relative to A; B then makes an initial approach and begins to hover with respect to A. Hovering continues for an appropriate amount of time. The orientation of B is changed so that the opening of the container is facing A, and angular velocity of B relative to A is eliminated. Descent takes place as $\hat{\mathbf{b}}_3$ remains collinear with a line fixed in A. The object of interest is collected in the container and made firmly attached to B; if A is a large asteroid, B must ascend from its surface. The final step involves arresting the angular velocity of the rigid body formed by B and its payload, denoted simply by B for convenience. Trajectory and attitude dynamics and control involved in each of these steps are examined in detail in Secs. 2–6 of the paper. Concluding remarks appear in Sec. 7.

2. Initial Approach

Our analysis of dynamics and control begins with the initial approach of the spacecraft from a point relatively close to the asteroid. In the interest of simplicity, the heliocentric orbit of the asteroid, A, is taken to be a circle of radius R, as shown in Fig. 2. Throughout the paper, A is treated as a rigid body, and the gravitational force exerted by A on the spacecraft is neglected. Rotational motion of A is modeled as torque-free, before it is captured.

Analysis is facilitated by introducing a right-handed set of mutually perpendicular unit vectors $\hat{\mathbf{L}}_1$, $\hat{\mathbf{L}}_2$, and $\hat{\mathbf{L}}_3$, fixed in a local-vertical-local-horizontal reference frame L, and directed as shown in Fig. 2. $\hat{\mathbf{L}}_3$ is in the direction of the position vector from $A^\star$, the mass center of A, to S, the Sun. $\hat{\mathbf{L}}_1$ is in the direction of the asteroid's orbital velocity or, more precisely, the velocity of $A^\star$ in a Newtonian reference frame N. Together, $\hat{\mathbf{L}}_1$ and $\hat{\mathbf{L}}_3$ define the plane of the heliocentric orbit.

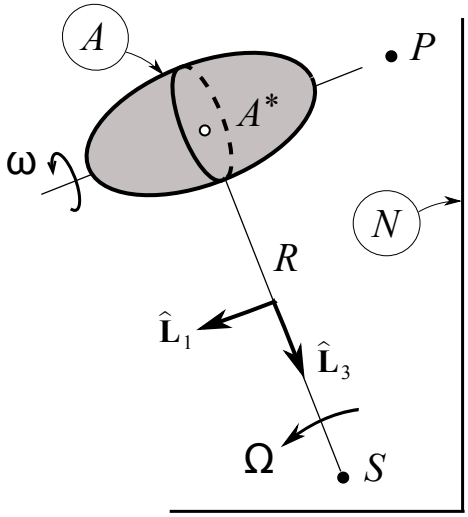

Figure 2: Asteroid in Circular Heliocentric Orbit

The angular velocity ${}^N\boldsymbol{\omega}^L$ of L in N is given by

$$ {}^N\boldsymbol{\omega}^L = -\Omega\,\hat{\mathbf{L}}_2 \tag{1}$$

where Ω is a positive constant, and $\hat{\mathbf{L}}_2$ is normal to the asteroid's orbit plane. The most general rotational motion of A that can be considered is tumbling; we expect, however, that it will prove difficult to carry out and present results of studies of approach, hover, descent, and ascent associated with a tumbling body. Consequently, we conduct a preliminary investigation by taking the angular velocity ${}^L\boldsymbol{\omega}^A$ of A in L to be

$$ {}^L\boldsymbol{\omega}^A = \omega\,\hat{\mathbf{L}}_1 \tag{2}$$

where ω is a positive constant. As is well known, the proposed rotational motion is not stable unless ${}^N\boldsymbol{\omega}^A = \omega\hat{\mathbf{L}}_1 - \Omega\hat{\mathbf{L}}_2$ is parallel to the central principal axis of inertia of A associated with the largest central principal moment of inertia, or the smallest. In what follows, we concern ourselves with intervals of time during which ${}^L\boldsymbol{\omega}^A$ satisfies Eq. (2). Furthermore, the equatorial plane of A is regarded as the $\hat{\mathbf{L}}_2$-$\hat{\mathbf{L}}_3$ plane, the direction of the North pole is $\hat{\mathbf{L}}_1$, and the direction of the South pole is $-\hat{\mathbf{L}}_1$.

Before it commences to approach A, the spacecraft is taken to be stationary in L at a point P, trailing the asteroid over its South pole as shown in Figs. 2 and 3. The approach trajectory ends in conditions that permit hovering to begin; in other words, the velocity of the spacecraft is such that it is fixed in reference frame (rigid body) A. In Fig. 3, Q belongs to a set of points on the surface of a sphere, D, whose radius exceeds the largest dimension of A. We investigate trajectories to points on the surface of D.

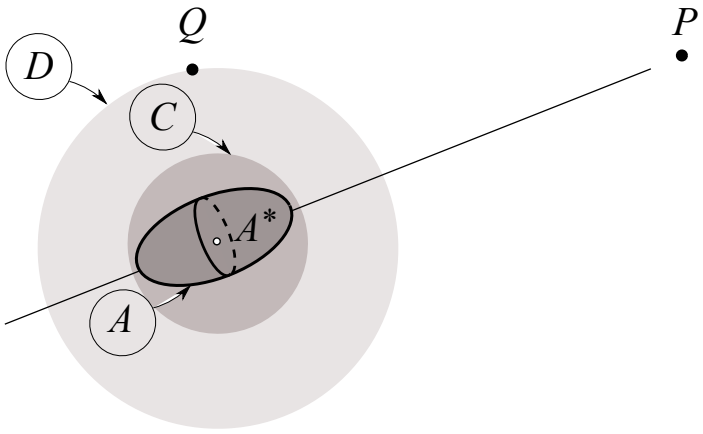

Figure 3: Hovering Stations and Collision Avoidance Constraint

The total velocity increment, ΔV, needed for each trajectory is minimized with an interior-point optimization algorithm that allows the trajectory to be constrained in order to avoid a collision with A. The constraint can be described as a simple geometric shape that envelops A; in this study, the shape is taken to be a sphere, denoted by C in Fig. 3. The algorithm is applied to translation governed by linearized equations of motion relative to a circular orbit, sometimes referred to as the Euler-Hill equations (see Ref. [3], p. 111). Here, we neglect terms in those equations representing perturbing forces acting on the spacecraft, such as gravitational attraction of the asteroid and solar radiation pressure.

The results that follow are obtained with $R = 0.9$ astronomical units (AU), which corresponds to $\Omega = 1.3 \times 10^{-5}$ deg/s. Each trajectory departs from P, 50 m behind $A^\star$. Time of flight is arbitrarily specified as 2600 s (43.3 minutes), which we believe to be a reasonable duration. The points on the surface of D at which each trajectory ends are at various latitudes and longitudes with respect to A; the radius of D is 20 m. The radius of C, the constraint or "keep-out" sphere, is set to 10 m. ω takes on values of 0.5, 1, 5, 10, and 60 rev/hr (rph).

Under the aforementioned conditions, trajectories ending over the southern hemisphere of A require two impulses: one to depart P, and one to yield a velocity such that the spacecraft can begin to hover at the desired point fixed in A. The radius of C is small enough that some trajectories ending over the northern hemisphere can be accomplished with two impulses. Other trajectories to stations over the northern hemisphere require three impulses.

As one might expect, for stations at a given latitude the required ΔV is virtually independent of the longitude. The results, therefore, can be presented for various values of latitude and ω, as seen in Fig. 4. Latitudes of $-90°$, $0°$, and $90°$ are associated, respectively, with points over the South pole ($-\hat{\mathbf{L}}_1$), equator, and North pole ($\hat{\mathbf{L}}_1$) (see Fig. 2). The left side of Fig. 4 contains plots of ΔV; the plots on the right side show the propellant mass, Δm, obtained from ΔV via the rocket equation $\Delta m = m_0[1 - e^{-\Delta V/(g\, I_{sp})}]$ with spacecraft mass $m_0 = 18,000$ kg, $I_{\text{sp}} = 287$ s, and $g = 9.8$ m/s^2.

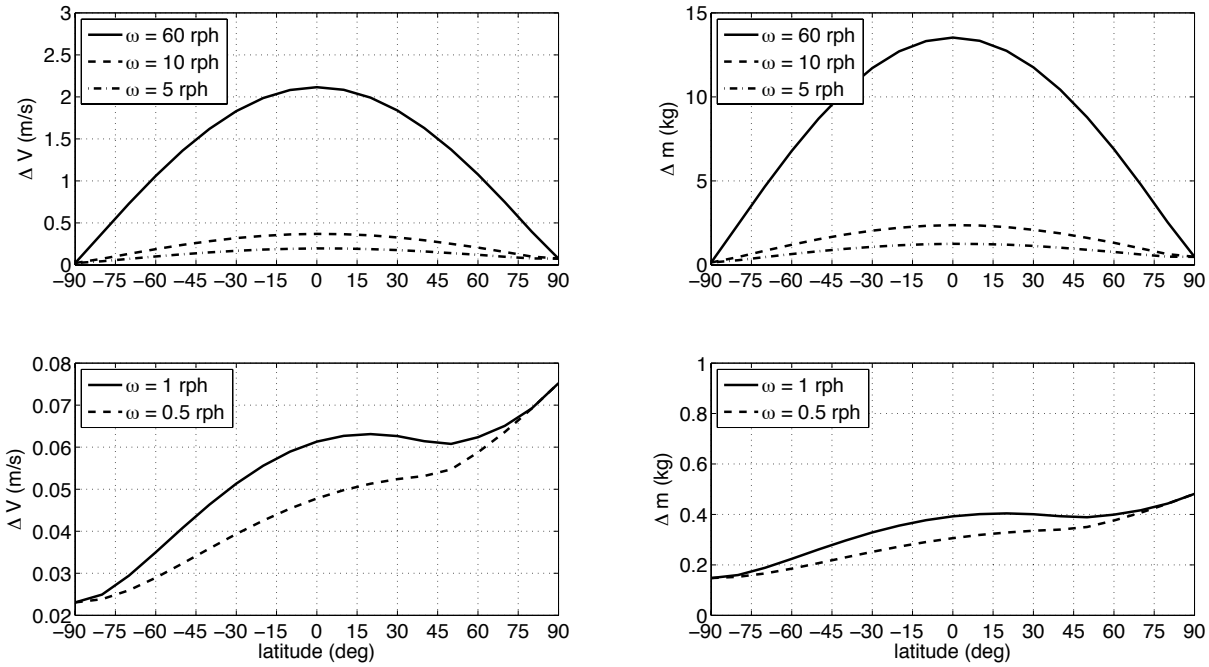

Figure 4: ΔV and Propellant Mass for Approach Trajectories

Results for stations directly over the poles are independent of ω; the two-impulse trajectory to the South pole requires $\Delta V = 0.023$ m/s and $\Delta m = 0.15$ kg, whereas the three-impulse trip to the North pole requires $\Delta V = 0.075$ m/s and $\Delta m = 0.48$ kg. For low spin rates, $\omega = 0.5$ and 1 rph, the trajectory to the North pole is more expensive than one to a point over the equator. On the other hand, reaching the hovering condition over the equator becomes the most expensive maneuver at the higher spin rates.

In the case of a small asteroid for which ${}^{L}\boldsymbol{\omega}^{A}$ satisfies Eq. (2), it is only necessary to consider approaching a point on the South or North pole. It is, however, worthwhile to consider approaching points at various latitudes because a suitable boulder may be resting on the surface of a large asteroid at any location.

3. Hover

The approach trajectories studied in Sec. 2 put the spacecraft in position to hover; however, propulsive force is required to maintain hover. A hovering spacecraft traces out in L a circle whose center is on the line that passes through $A^\star$ and is parallel to $\hat{\mathbf{L}}_1$ (see Fig. 2). The plane of the circle is parallel to the $\hat{\mathbf{L}}_2$-$\hat{\mathbf{L}}_3$ plane. Because the stations of interest lie on the surface of D centered at $A^\star$ (see Fig. 3), the radius ρ of the circle can be written as

$$\rho = H\cos\lambda \tag{3}$$

where H is the radius of D, and where λ is the latitude of the station. Thus, for a spacecraft regarded as a particle Q hovering at a station that is initially in the plane of the asteroid's orbit and on the same side of $A^\star$ as the Sun, the position vector from $A^\star$ to Q can be expressed as a function of time t,

$$\mathbf{r}^{A^\star Q} = H\sin\lambda\hat{\mathbf{L}}_1 + H\cos\lambda(-\sin\omega t\hat{\mathbf{L}}_2 + \cos\omega t\hat{\mathbf{L}}_3) \tag{4}$$

From this relationship one can obtain quantities appearing in the Euler-Hill equations,

$$x \triangleq \mathbf{r}^{A^\star Q}\cdot\hat{\mathbf{L}}_1 = H\sin\lambda \qquad y \triangleq \mathbf{r}^{A^\star Q}\cdot\hat{\mathbf{L}}_2 = -H\cos\lambda\sin\omega t \qquad z \triangleq \mathbf{r}^{A^\star Q}\cdot\hat{\mathbf{L}}_3 = H\cos\lambda\cos\omega t \tag{5}$$

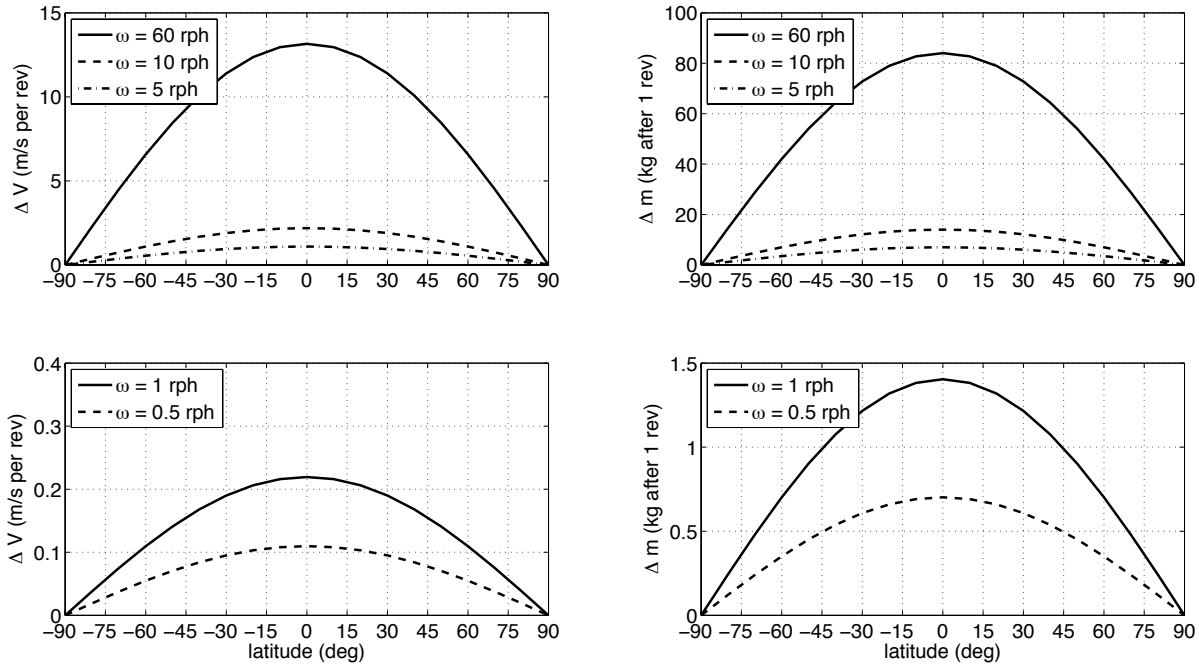

Figure 5: ΔV and Propellant Mass for Hovering

and the Euler-Hill equations can then be written as

$$\ddot{x} - 2\Omega\dot{z} = 2H\Omega\omega\cos\lambda\sin\omega t = \mathbf{f}\cdot\hat{\mathbf{L}}_1 \tag{6}$$

$$\ddot{y} + \Omega^2 y = H(\omega^2 - \Omega^2)\cos\lambda\sin\omega t = \mathbf{f}\cdot\hat{\mathbf{L}}_2 \tag{7}$$

$$\ddot{z} + 2\Omega\dot{x} - 3\Omega^2 z = -H(\omega^2 + 3\Omega^2)\cos\lambda\cos\omega t = \mathbf{f}\cdot\hat{\mathbf{L}}_3 \tag{8}$$

where $\mathbf{f}$ is the resultant force per unit mass acting on Q, other than the gravitational attraction of the Sun. The smallest value of ω presently under consideration is 5×10^{-2} deg/s, whereas $\Omega = 1.3\times10^{-5}$ deg/s. Therefore, in comparison to terms involving ω^2, one can neglect terms involving Ω and Ω^2. Thus, after multiplying Eqs. (7) and (8) by $\sin\omega t$ and $-\cos\omega t$, respectively, and adding the results, one obtains

$$H\omega^2\cos\lambda = \mathbf{f}\cdot(\sin\omega t\hat{\mathbf{L}}_2 - \cos\omega t\hat{\mathbf{L}}_3) = -\mathbf{f}\cdot\hat{\mathbf{a}}_3 \tag{9}$$

where unit vector $\hat{\mathbf{a}}_3$ is fixed in A and has the same direction as $\hat{\mathbf{L}}_3$ at $t = 0$. This result tells us that hovering can essentially be accomplished by applying propulsive force per unit mass $\mathbf{f}$ directed toward the spin axis of A, along a line passing through Q and perpendicular to the spin axis. It is therefore advisable for the orientation of the spacecraft to be such that a pair (or two) of thrusters can apply thrust in the direction of $-\hat{\mathbf{a}}_3$.

Letting $\hat{\mathbf{a}}_1$ and $\hat{\mathbf{a}}_2$ be unit vectors fixed in A such that $\hat{\mathbf{a}}_1 = \hat{\mathbf{L}}_1$, and $\hat{\mathbf{a}}_2$ has the same direction as $\hat{\mathbf{L}}_2$ at $t = 0$, one can express the velocity increments needed to maintain hovering for one revolution of A as

$$\Delta V_r \triangleq \int_{t=0}^{t=2\pi/\omega} |\mathbf{f}\cdot\hat{\mathbf{a}}_r|\,dt \qquad (r = 1,2,3) \tag{10}$$

$$\Delta V_1 = 8\Omega H\cos\lambda \qquad \Delta V_2 = \frac{8}{\omega}\Omega^2 H\cos\lambda \qquad \Delta V_3 = \frac{2\pi}{\omega}(\omega^2+\Omega^2)H\cos\lambda \tag{11}$$

The total velocity increment $\Delta V = \Delta V_1 + \Delta V_2 + \Delta V_3$ ($\Delta V_3 \approx \Delta V$) required to hover for one revolution of A is plotted on the left side of Fig. 5 for various values of and ω and latitude, λ. The plots on the right side show the propellant mass, Δm, obtained from ΔV via the rocket equation with spacecraft mass $m_0 = 18,000$ kg, $I_{\rm sp} = 287$ s, and $g = 9.8$ m/s^2. Although Eqs. (11) are developed for stations that at $t = 0$ lie in the orbit plane of A, they are nevertheless applicable to all stations that share a common longitude because the integration in Eqs. (10) is performed over a complete revolution of A. Figure 5 indicates that pole-sitting can be accomplished without any effort whatsoever, which is to be expected because the polar axis of A is assumed to remain parallel to $\hat{\mathbf{L}}_1$, and the stations over the poles are in the orbit plane of A at the same heliocentric distance as $A^\star$. Figure 5 also shows that hovering comes at a cost that increases proportionally with ω. A comparison of Figs. 4 and 5 shows that hovering for one revolution is more expensive than the initial approach, unless the station is very near a pole. It is important to keep in mind that for, say, $\omega = 1$ rev/hr the associated curve for ΔV in Fig. 5 shows what is required to hover for one hour, whereas the curve for ΔV corresponding to $\omega = 60$ rev/hr must be scaled by a factor of 60 to determine what is required for one hour of hovering. Consequently, hovering can require prohibitive amounts of propellant when ω is large.

4. Removal of Relative Angular Velocity

Following a period of time during which hovering is performed, as discussed in Sec. 3, the spacecraft's attitude and angular velocity are altered to prepare for collection of the object of interest. We assume the method of collection requires that there be no relative angular velocity between the asteroid and the spacecraft when the two make contact. Letting B denote the spacecraft, one can express this condition as ${}^A\boldsymbol{\omega}^B = \mathbf{0}$, where ${}^A\boldsymbol{\omega}^B$ is the angular velocity of B in A. The condition can also be expressed as ${}^A\boldsymbol{\omega}^B = {}^N\boldsymbol{\omega}^B - {}^N\boldsymbol{\omega}^A = \mathbf{0}$, where ${}^N\boldsymbol{\omega}^A$ and ${}^N\boldsymbol{\omega}^B$ are, respectively, the angular velocities of A and B in a Newtonian reference frame N. Clearly, a control system cannot be used to make ${}^N\boldsymbol{\omega}^B$ equal to ${}^N\boldsymbol{\omega}^A$ unless ${}^N\boldsymbol{\omega}^A$ is a known function of time.

The reader will recall that we treat rotational motion of A in N as torque-free. When the orientation of A in N, and the values of ${}^N\boldsymbol{\omega}^A \cdot \hat{\mathbf{a}}_r$ ($r = 1, 2, 3$), are specified at a particular time t_0, one can then produce a time history of ${}^N\boldsymbol{\omega}^A$ in a number of ways. (In practice the orientation and ${}^N\boldsymbol{\omega}^A$ at t_0 are determined from measurements made with sensors placed on B.) The first of these is numerical integration of Euler's dynamical equations together with a set of kinematical differential equations governing parameters suitable for describing the orientation of A in N. That is the approach we take in this work. Alternatively, closed-form solutions for ${}^N\boldsymbol{\omega}^A \cdot \hat{\mathbf{a}}_r$ ($r = 1, 2, 3$) are available in terms of Jacobian elliptic functions when A is unsymmetric; that is, when it has three distinct central principal moments of inertia (see Ref. [4], Sec. 3.4). In the special case of two identical central principal moments of inertia, A is axisymmetric and its angular velocity can be described simply in terms of spin about the axis of symmetry, together with precession about the angular momentum vector (see Ref. [4], Sec. 3.1).

As mentioned previously, we regard spacecraft B as an axisymmetric rigid body. We assume that operation of the capture mechanism requires the axis of symmetry of B to be collinear with a line of descent fixed in asteroid A, but that effective use of the mechanism does not require any particular relative orientation, about the symmetry axis, between B and A.

In Ref. [5], Tsiotras and Longuski address the problem of controlling B while it performs simple rotational motion in N about $\hat{\mathbf{b}}_3$, a unit vector parallel to the axis of symmetry. The objective is for $\hat{\mathbf{b}}_3$ to have the same direction as $\hat{\mathbf{n}}$, a unit vector fixed in N. They use two parameters to represent the direction of $\hat{\mathbf{n}}$ in B, and develop a globally asymptotically stable control algorithm. We have extended their work to develop a "spin-up" feedback controller that drives $\hat{\mathbf{b}}_3$ to the same direction as $\hat{\mathbf{a}}$, a unit vector fixed in A and parallel to the line of descent, and also drives ${}^A\boldsymbol{\omega}^B$ to $\mathbf{0}$. Whereas control is accomplished in Ref. [5] with torque applied in two directions, our objectives in general require three-axis control.

A specific procedure is now described. We begin by identifying a line of descent fixed in A, and letting $\hat{\mathbf{a}}$ be a unit vector parallel to this line. Predictions are made as to the direction of $\hat{\mathbf{a}}$ in N at some future time t^*, as well as the value of ${}^N\boldsymbol{\omega}^A \cdot \hat{\mathbf{a}}$ at t^*. An initial reorientation of B is performed to bring $\hat{\mathbf{b}}_3$ to the predicted direction of $\hat{\mathbf{a}}$ in N. Provided ${}^N\boldsymbol{\omega}^B = \mathbf{0}$ before the reorientation begins, the change in the attitude

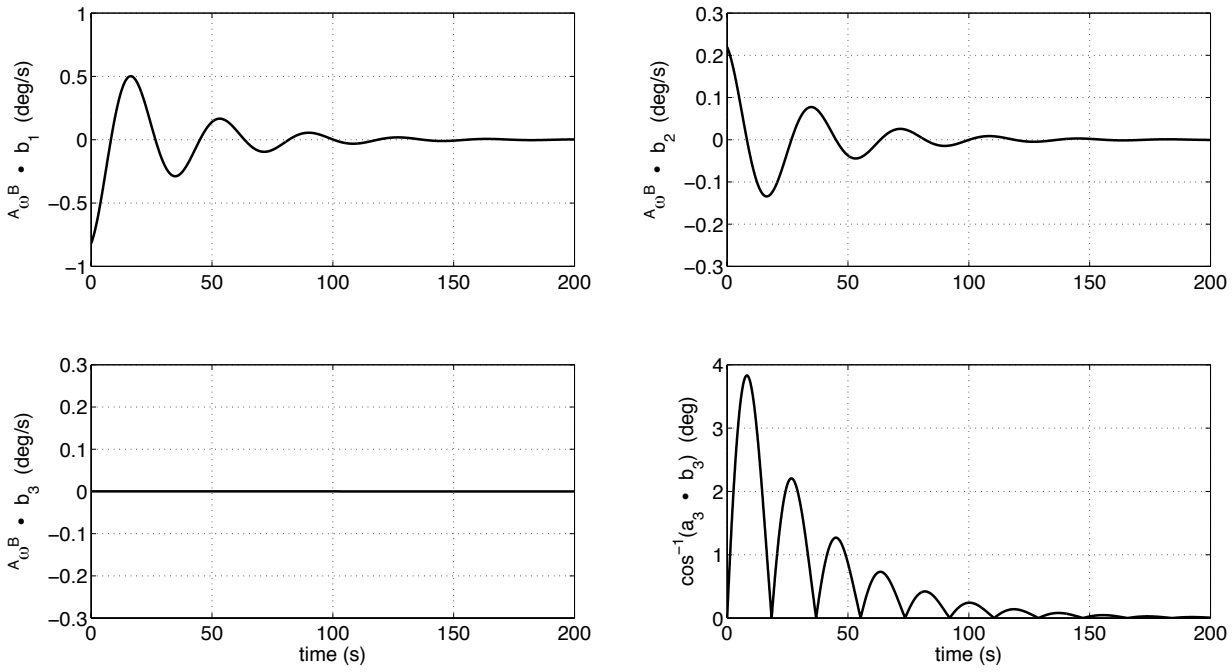

Figure 6: Relative Angular Velocity and Alignment of Axis of Symmetry During Spin-up

of B can be brought about slowly, by briefly firing RCS jets at the beginning and end of the maneuver, so that only a small amount of propellant is expended. (When the cost of hovering is high, it may be advisable to perform this slow maneuver before hovering begins.) Next, ${}^N\boldsymbol{\omega}^B \cdot \hat{\mathbf{b}}_3$ is made to have the predicted value of ${}^N\boldsymbol{\omega}^A \cdot \hat{\mathbf{a}}$. Finally, at time $t = t^*$ the feedback controller is employed to bring ${}^A\boldsymbol{\omega}^B$ to $\mathbf{0}$, and to give $\hat{\mathbf{b}}_3$ the same direction as $\hat{\mathbf{a}}$. Even though the motion of A is torque-free, control torque must be applied continuously to B to keep ${}^A\boldsymbol{\omega}^B = \mathbf{0}$.

Use of the feedback controller is demonstrated in an example involving an unsymmetric asteroid, taken to be an ellipsoid with semidiameters $a = 5$ m, $b = 3$ m, and $c = 4$ m, a uniform density of 2000 kg/m^3, and therefore a mass of 502.65×10^3 kg. If we take $\hat{\mathbf{a}}_1$, $\hat{\mathbf{a}}_2$, and $\hat{\mathbf{a}}_3$ to be parallel to central principal axes of inertia of A, then the associated central principal moments of inertia are, respectively, $J_1 = 2.52 \times 10^6$ kg-m^2, $J_2 = 4.13 \times 10^6$ kg-m^2, and $J_3 = 3.42 \times 10^6$ kg-m^2. The angular velocity of A in N is characterized at $t = t^* = 0$ by the values ${}^N\boldsymbol{\omega}^A \cdot \hat{\mathbf{a}}_1 = 0.6$ deg/s, ${}^N\boldsymbol{\omega}^A \cdot \hat{\mathbf{a}}_2 = 0.6$ deg/s, and ${}^N\boldsymbol{\omega}^A \cdot \hat{\mathbf{a}}_3 = 6.0$ deg/s (60 rph). Unit vectors $\hat{\mathbf{n}}_1$, $\hat{\mathbf{n}}_2$, and $\hat{\mathbf{n}}_3$ fixed in N can always be chosen such that $\hat{\mathbf{n}}_r = \hat{\mathbf{a}}_r$ $(r = 1, 2, 3)$ at $t = t^* = 0$. The line of descent is chosen to be parallel to $\hat{\mathbf{a}}_3$.

According to the procedure previously described, an initial reorientation of B brings $\hat{\mathbf{b}}_3$ to the direction $\hat{\mathbf{a}}_3$ is predicted to have at $t = t^* = 0$, and the required propellant mass is assumed to be negligible. At the conclusion of the reorientation, ${}^N\boldsymbol{\omega}^B = \mathbf{0}$. Next, four RCS thrusters (see Table 1) are used to apply a couple whose torque is given by $\mathbf{T} = 1600\,\hat{\mathbf{b}}_3$ Nm; ${}^N\boldsymbol{\omega}^B \cdot \hat{\mathbf{b}}_3$ reaches the required value of 6.0 deg/s in 1.07 s, and 0.31 kg of propellant is consumed in the process. To emphasize that the relative orientation about $\hat{\mathbf{b}}_3$ between B and A can be arbitrary, we assume the angle between $\hat{\mathbf{a}}_1$ and $\hat{\mathbf{b}}_1$ (which is the same as the angle between $\hat{\mathbf{a}}_2$ and $\hat{\mathbf{b}}_2$) is 60° at $t = t^* = 0$. At this time the feedback controller is employed, and the resulting motion of B relative to A is shown in Fig. 6. Plots of ${}^A\boldsymbol{\omega}^B \cdot \hat{\mathbf{b}}_r$ $(r = 1, 2, 3)$ appear respectively in the upper left, upper right, and lower left of Fig. 6; in the first two cases, the controller drives the errors to zero in approximately 200 s, whereas in the third case the controller is able to maintain an error of zero.

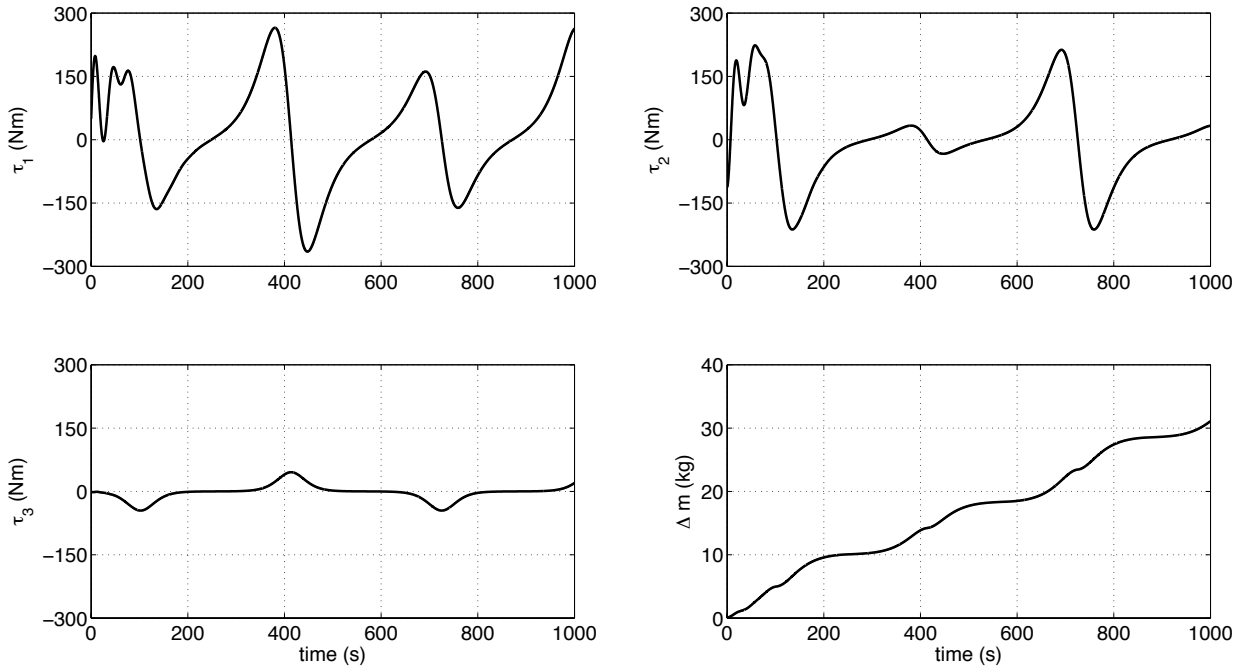

Figure 7: Control Torque and Propellant Mass for Spin-up

The angle between $\hat{\mathbf{b}}_3$ and $\hat{\mathbf{a}}_3$, which can be expressed as $\cos^{-1}(\hat{\mathbf{a}}_3 \cdot \hat{\mathbf{b}}_3)$, is plotted in the lower right of Fig. 6. The controller keeps this angle less than 4 deg, and drives the angle to zero within 200 s.

Control torque must be applied continuously to B to keep ${}^A\boldsymbol{\omega}^B = \mathbf{0}$ for $t > 200$ s, as can be seen in Fig. 7. Time histories of $\tau_r \triangleq \mathbf{T} \cdot \hat{\mathbf{b}}_r$ $(r = 1, 2, 3)$, where $\mathbf{T}$ is the control torque exerted by the RCS on B, are shown respectively in the upper left, upper right, and lower left of Fig. 7. The torque needed to synchronize rotational motion of B with A is large because the asteroid is tumbling at high angular speed. The propellant mass Δm consumed by the RCS thrusters, shown in the lower right of Fig. 7, reaches 31 kg after 1000 s. It is important to note that this expenditure of propellant gives $\hat{\mathbf{b}}_3$ the same direction as $\hat{\mathbf{a}}_3$, which is parallel to the line of descent; additional propellant is required, however, to make B translate such that $\hat{\mathbf{b}}_3$ and the line of descent fixed in A remain collinear.

5. Descent and Ascent

After ${}^A\boldsymbol{\omega}^B$ has been brought to $\mathbf{0}$ and $\hat{\mathbf{b}}_3$ has been given the direction of a line of descent fixed in A, as discussed in Sec. 4, B can begin to descend in the direction of $\hat{\mathbf{b}}_3$ towards A. When A is a large asteroid and a small boulder is to be collected from its surface, B must ascend after the payload is secured. Beginning from a condition of hover, descent is initiated with an impulsive velocity increment. Likewise, descent is terminated and B is brought to rest in A by an impulsive change in velocity. During the descent, thrust must be applied continuously to keep B from moving relative to A in any direction normal to the line of descent. Ascent is regarded as descent in reverse.

In what follows we consider an asteroid moving as described in Sec. 2, and report ΔV and corresponding propellant mass Δm for descent and ascent. These quantities are functions of latitude of the line of descent, time of flight, and ω [see Eq. (2)].

In examining descent, we regard A as sphere with a radius of 3.5 m. Each descent begins from a point 20 m distant from $A^\star$, and ends at a point on the surface of A, 3.5 m from $A^\star$. In each case, the line of

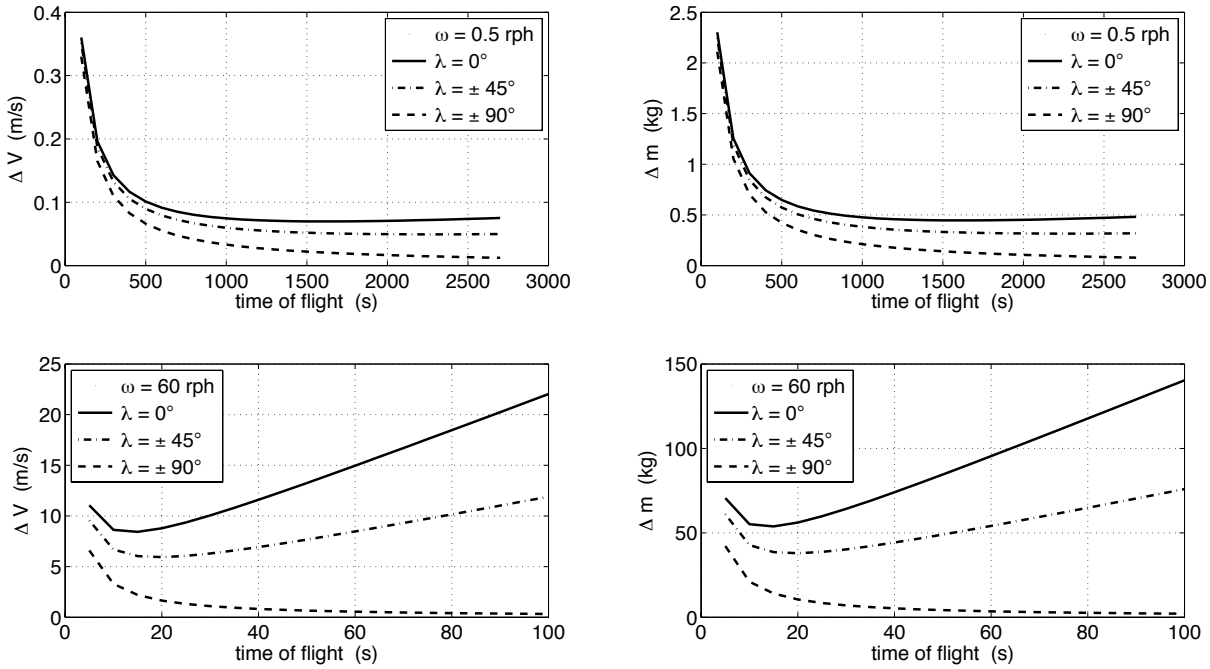

Figure 8: ΔV and Propellant Mass for Descent

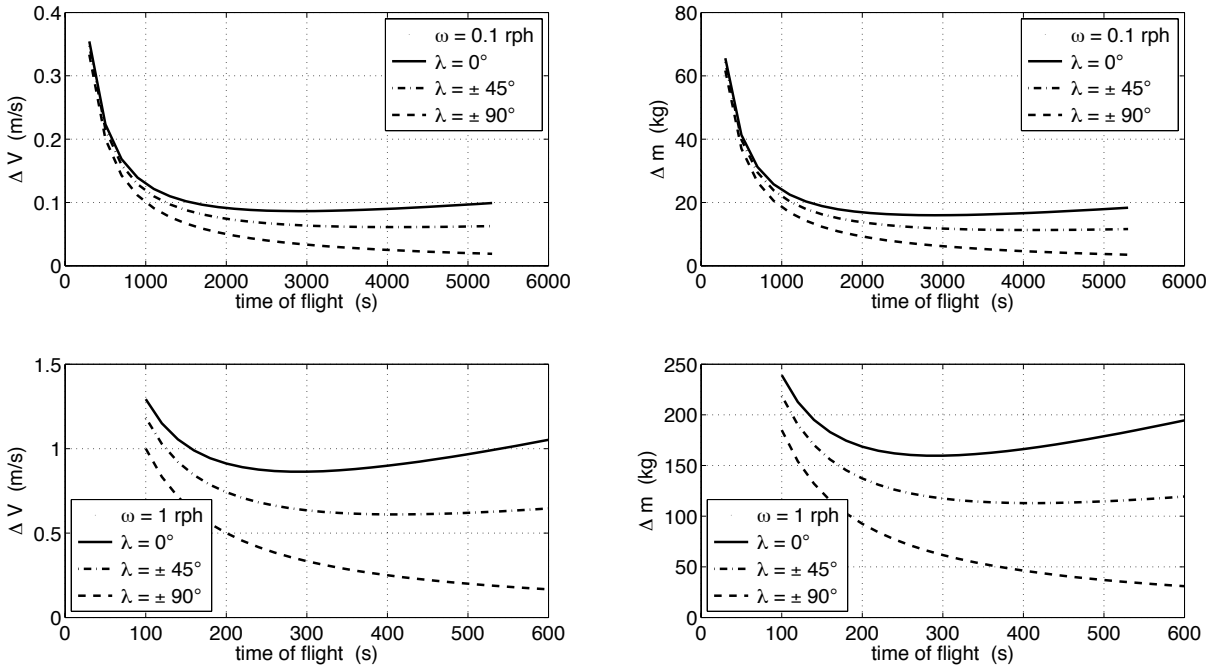

Figure 9: ΔV and Propellant Mass for Ascent

descent is taken to be normal to the surface of A. The left side of Fig. 8 contains plots of ΔV; the plots on the right side show the propellant mass, Δm, obtained from ΔV via the rocket equation with spacecraft mass $m_0 = 18,000$ kg, $I_{\text{sp}} = 287$ s, and $g = 9.8$ m/s^2. Results correspond to $\omega = 0.5$ rph on the top, and to $\omega = 60$ rph on the bottom. (Although we also obtained results for $\omega = 1$, 5, and 10 rph, they are omitted in the interest of brevity.) The three curves in each plot correspond to values of latitude $\lambda = 0°$ (solid), $\pm 45°$ (dash-dot), and $\pm 90°$ (dash); results are independent of the sign of λ, as is the case with results for hovering shown in Fig. 5.

Time of flight (the duration of descent) ranges from 100 s to 2700 s in the case of $\omega = 0.5$ rph, and from 5 s to 100 s in the case of $\omega = 60$ rph. The ranges are selected so as to illustrate the presence of minima in some of the curves; descending too quickly or too slowly can be expensive. Optimal times of flight for $\omega = 60$ rph are markedly shorter than those for $\omega = 0.5$ rph; although a rapid descent can save a significant amount of propellant, it may not be operationally prudent. For a given value of ω, descending to the equator is more expensive than descending to any other latitude. Conversely, descending to either pole is the least expensive; in fact, descent along the polar axis is independent of ω. For this reason, the curves associated with $\lambda = \pm 90°$ on the top and bottom of Fig. 8 are two parts of the same curve, which decreases monotonically.

To study ascent, we treat A as a sphere having a radius of 250 m. Each ascent begins from a point on the surface of A, proceeds along a line of ascent fixed in A and normal to the surface, and ends at distance of 300 m from $A^\star$ (in other words, at an altitude of 50 m).

The left side of Fig. 9 contains plots of ΔV. Because larger asteroids are thought to rotate more slowly in general than smaller ones, we allow ω to take on the values of 0.1 rph (top), and 1 rph (bottom). For convenience, the boulder to be collected is taken to be the object studied in Sec. 4; its mass is 502.65×10^3 kg. Thus, the spacecraft and payload together have a mass of 520.65×10^3 kg, and this is the value of m_0 used in the rocket equation to obtain the curves plotted on the right hand side of Fig. 9.

6. Removal of Inertial Angular Velocity

After a small asteroid has been secured in the container of B, or after a small boulder has been collected and B has ascended from the surface of a large asteroid, ${}^N\boldsymbol{\omega}^B$ is made to vanish. This is considered necessary, for example, to orient solar arrays properly or to aim thrust in the direction needed to return to the Earth-Moon system. We assume that the spacecraft and its payload now form one rigid body. For convenience B will denote the newly formed rigid body, henceforth regarded as unsymmetric in order to maintain generality.

In this section we develop an asymptotically stable control algorithm for applying torque to drive ${}^N\boldsymbol{\omega}^B$ to $\mathbf{0}$. No requirements are placed on the orientation of B in N at the time ${}^N\boldsymbol{\omega}^B$ reaches $\mathbf{0}$; the required orientation can subsequently be obtained by briefly firing RCS thrusters at the beginning and end of a slow reorientation that consumes a negligible amount of propellant. The controller is exercised with an example taken from Ref. [1].

Euler's dynamical equations of motion for a rigid body B can be written as

$$\underline{\mathbf{I}} \cdot {}^N\boldsymbol{\alpha}^B = \mathbf{T} - {}^N\boldsymbol{\omega}^B \times \underline{\mathbf{I}} \cdot {}^N\boldsymbol{\omega}^B \tag{12}$$

where $\underline{\mathbf{I}}$ is the central inertia dyadic of B, ${}^N\boldsymbol{\alpha}^B$ is the angular acceleration of B in a Newtonian reference frame N, and $\mathbf{T}$ is the moment about $B^\star$, the mass center of B, of external forces acting on B. The rotational kinetic energy K of B in N can be written as

$$K = \tfrac{1}{2}\, {}^N\boldsymbol{\omega}^B \cdot \underline{\mathbf{I}} \cdot {}^N\boldsymbol{\omega}^B \tag{13}$$

Hence, the time rate of change of K is given by

$$\dot{K} = {}^N\boldsymbol{\omega}^B \cdot \underline{\mathbf{I}} \cdot {}^N\boldsymbol{\alpha}^B = {}^N\boldsymbol{\omega}^B \cdot \left(\mathbf{T} - {}^N\boldsymbol{\omega}^B \times \underline{\mathbf{I}} \cdot {}^N\boldsymbol{\omega}^B\right) = {}^N\boldsymbol{\omega}^B \cdot \mathbf{T} \tag{14}$$

Because the vector product of ${}^N\boldsymbol{\omega}^B$ and the vector $\underline{\mathbf{I}} \cdot {}^N\boldsymbol{\omega}^B$ is necessarily perpendicular to ${}^N\boldsymbol{\omega}^B$, the scalar product of ${}^N\boldsymbol{\omega}^B$ and ${}^N\boldsymbol{\omega}^B \times \underline{\mathbf{I}} \cdot {}^N\boldsymbol{\omega}^B$ necessarily vanishes.

In order to drive ${}^N\boldsymbol{\omega}^B$ to $\mathbf{0}$, we seek a strategy for applying control torque $\mathbf{T}$ that will dissipate rotational kinetic energy; that is, we wish to have $\dot{K} < 0$. At the same time, we seek to apply torque sparingly so as to avoid excessive expenditure of propellant. These considerations lead us to an objective function J defined as

$$J \triangleq \omega^T \tau + \tfrac{1}{2}\tau^T R \tau \tag{15}$$

where ω is a 3×1 column matrix whose elements are ${}^N\boldsymbol{\omega}^B \cdot \hat{\mathbf{b}}_r$, τ is a 3×1 column matrix whose elements are $\mathbf{T} \cdot \hat{\mathbf{b}}_r$ $(r = 1, 2, 3)$, R is a 3×3 positive definite matrix, and where a superscript T denotes matrix transposition. Forming the matrix product $\omega^T \tau$ yields the same result as forming the scalar product ${}^N\boldsymbol{\omega}^B \cdot \mathbf{T}$, namely the time rate of change of rotational kinetic energy. The matrix product $\frac{1}{2}\tau^T R \tau$ is referred to as control energy. The matrix τ for which J is a minimum can be found by setting the partial derivative of J with respect to τ equal to zero,

$$\omega^T + \tau^T R = 0 \tag{16}$$

whereupon we find

$$\tau = -R^{-1}\omega \tag{17}$$

and

$$\dot{K} = -\omega^T R^{-1} \omega \tag{18}$$

Because R is positive definite (therefore, so is R^{-1}), $\dot{K} \leq 0$. Moreover, $\dot{K} = 0$ if and only if $\omega = 0$. Thus, according to Lyapunov theory (Ref. [6]), τ as given by Eqs. (17) provides asymptotically stable control of the system governed by Eqs. (12). Numerical values of the elements of R can be adjusted to trade the use of control energy for dissipation of rotational kinetic energy: higher values result in smaller control torque and slower dissipation of energy, whereas lower values lead to larger control torque and faster energy dissipation.

An example in Ref. [1] (p. 35) involves an asteroid modeled as a cylinder with a radius of 3 m, a height of 12 m, and a mass of 1.1×10^6 kg. The cylinder's axis of symmetry is taken to be parallel to unit vector $\hat{\mathbf{b}}_1$ fixed in the spacecraft; thus, central principal moments of inertia of the asteroid for $\hat{\mathbf{b}}_1$, $\hat{\mathbf{b}}_2$, and $\hat{\mathbf{b}}_3$ are, respectively, $J_1 = 4.95 \times 10^6$ kg-m^2, and $J_2 = J_3 = 15.675 \times 10^6$ kg-m^2. Keeping in mind that the height of the spacecraft is 5.9 m and the radius of the asteroid is 3 m, the position vector from the spacecraft mass center to the asteroid mass center is given by $5.95\,\hat{\mathbf{b}}_3$ m, and the central principal moments of inertia of B for $\hat{\mathbf{b}}_1$, $\hat{\mathbf{b}}_2$, and $\hat{\mathbf{b}}_3$ are $K_1 = 0.5673 \times 10^7$ kg-m^2, $K_2 = 1.6398 \times 10^7$ kg-m^2, and $K_3 = 1.5691 \times 10^7$ kg-m^2. Evidently B is unsymmetric as the values of K_1, K_2, and K_3 are distinct. Angular velocity is taken to be ${}^N\boldsymbol{\omega}^B = 6\,\hat{\mathbf{b}}_3$ deg/s. It naturally occurs to an analyst to use the thrusters described in Table 1 to apply force in the form of a couple whose torque has the same direction as $-\hat{\mathbf{b}}_3$, in which case the moment arms are 2 m. The authors of Ref. [1] take such an approach and determine that bringing ${}^N\boldsymbol{\omega}^B$ to $\mathbf{0}$ consumes 306 kg of propellant. (The value is 292 kg according to our calculations).

We now show it is possible to use substantially less than 300 kg of propellant to arrest the rotational motion of B. After referring to Table 1 one can observe that, without the asteroid, $\mathbf{r}^{B^\star P_r} \cdot \hat{\mathbf{b}}_3 = -2.65$ m. More importantly, with the asteroid in place, the value becomes $\mathbf{r}^{B^\star P_r} \cdot \hat{\mathbf{b}}_3 = -8.33$ m. This moment arm is more than 4 times longer than 2 m; there is a corresponding improvement in efficiency if thrusters can be employed so as to take advantage of the longer moment arm. To bring the longer moment arm into play, one must first forgo application of thruster forces in couples. As will be demonstrated presently, in the current example one can ignore the consequences of applying thruster forces with a non-zero resultant. Moments about $B^\star$ of thruster forces applied with the 8.33-meter moment arm are necessarily perpendicular to $\hat{\mathbf{b}}_3$, whereas moments parallel to $\hat{\mathbf{b}}_3$ are necessarily applied with 2-meter moment arms. Consequently, it might at first appear that the long moment arm cannot be used to advantage in this case because the central angular momentum of B in N has the same direction as $\hat{\mathbf{b}}_3$. However, $\hat{\mathbf{b}}_3$ is parallel to the axis associated with the intermediate central principal moment of inertia, K_3, and rotational motion about such an axis is known to be unstable. It is possible, therefore, to exert torque briefly in a direction perpendicular to $\hat{\mathbf{b}}_3$ and intentionally induce instability to obtain tumbling motion; during the ensuing torque-free motion of the unsymmetric rigid body, the direction of angular momentum in B changes dramatically. When the angular momentum becomes nearly perpendicular to $\hat{\mathbf{b}}_3$, the long moment arms can be brought to bear. (It is worth

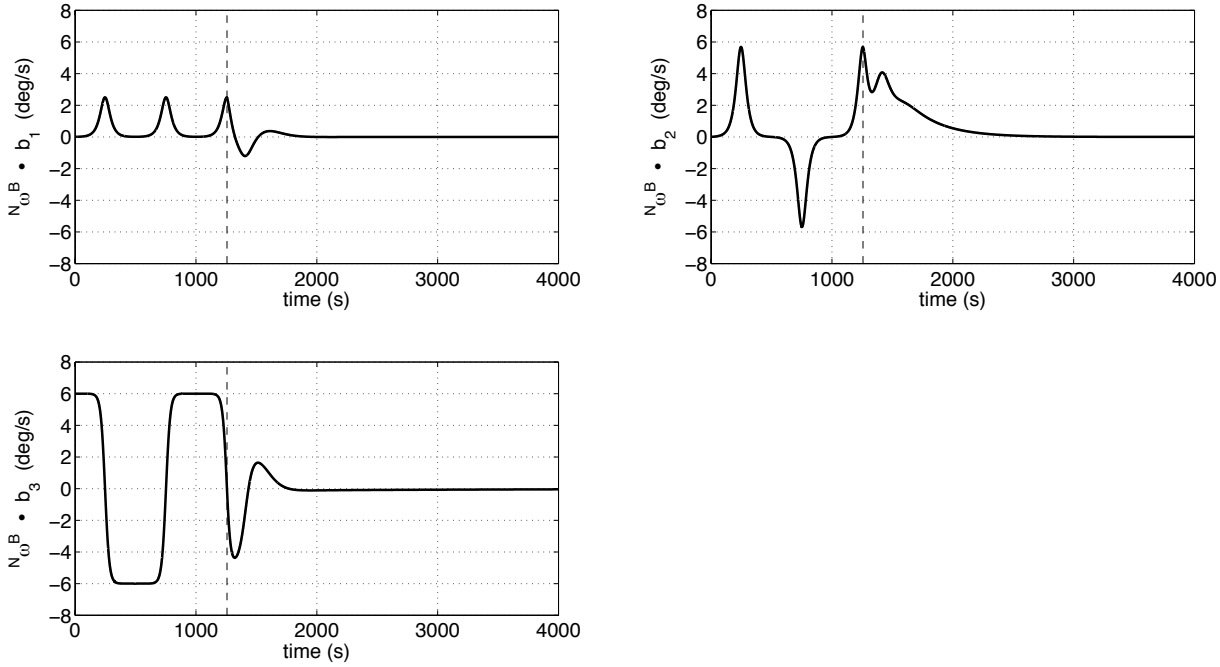

Figure 10: Angular Velocity During Despin

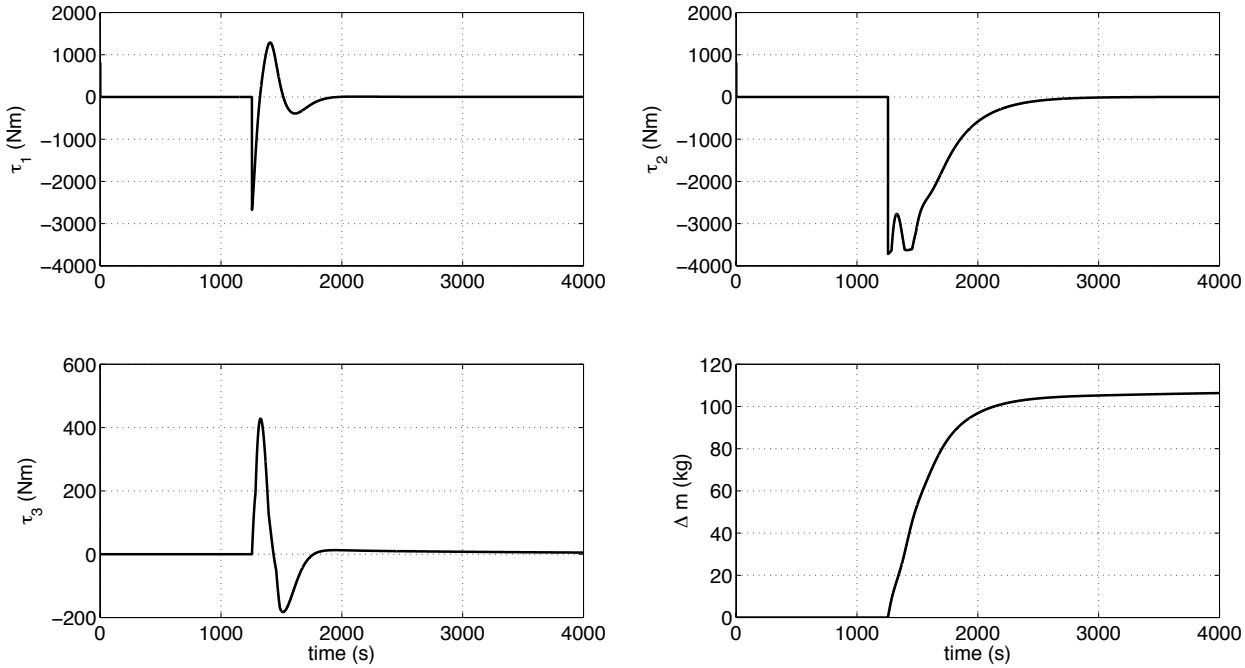

Figure 11: Control Torque and Propellant Mass for Despin

keeping in mind that this approach could not have been used if, in this example, ${}^N\boldsymbol{\omega}^B$ were parallel either to $\hat{\mathbf{b}}_1$ or to $\hat{\mathbf{b}}_2$, because in each case the rotational motion would be stable. Furthermore, this approach cannot be used when B is axisymmetric because in that case a small change in angular momentum cannot lead to tumbling.)

Figures 10 and 11 display the results of inducing tumbling, waiting for the central angular momentum of B to become perpendicular to $\hat{\mathbf{b}}_3$, and then engaging the asymptotically stable control given by Eqs. (17). At time $t = 0$, the central angular momentum of B in N is given by $\mathbf{H} = \underline{\mathbf{I}} \cdot {}^N\boldsymbol{\omega}^B = 1.6432 \times 10^6\,\hat{\mathbf{b}}_3$ Nms. Torque given by $\mathbf{T} = 800\,\hat{\mathbf{b}}_1 + 800\,\hat{\mathbf{b}}_2$ Nm is applied for 1 s. During the subsequent torque-free motion, ${}^N\boldsymbol{\omega}^B \cdot \hat{\mathbf{b}}_3$ becomes zero three times as can be seen in the lower left of Fig. 10, with the last of these instances occurring at $t = 1256.5$ s at which time the controller is activated. Vertical dashed lines indicate $t = 1256.5$ s in Fig. 10, and this instant is immediately obvious in Fig. 11. Control could have commenced the first or second time ${}^N\boldsymbol{\omega}^B \cdot \hat{\mathbf{b}}_3$ reached zero; the third instance was chosen in order to illustrate periodic torque-free rotational motion that takes place after perturbing torque has been applied. The matrix R is taken to be diagonal with all three elements equal to 100. Rotational motion of B is essentially arrested by $t = 2500$ s, which is 1250 s after control begins. Time histories of $\tau_r \triangleq \mathbf{T} \cdot \hat{\mathbf{b}}_r$ $(r = 1, 2, 3)$ are shown respectively in the upper left, upper right, and lower left of Fig. 11. Maximum magnitudes of τ_1 and τ_2 are larger than that of τ_3 by about a factor of 10. Propellant mass Δm consumed by the thrusters is shown in the lower right of Fig. 11 and it amounts to 108 kg, which represents a savings of 184 kg.

The reduction in RCS propellant consumption may come at the expense of a disruption to the orbital trajectory because the resultant thrust force is not zero. This possibility, however, is in general mitigated to a large extent because the trajectory is normally controlled by means of a solar electric propulsion (SEP) system having an $I_{\text{sp}} = 3000$ s, which greatly exceeds the 287-s I_{sp} of the RCS. Another mitigating factor is that rotational motion may allow RCS forces to cancel themselves to some extent as ${}^N\boldsymbol{\omega}^B$ is brought to $\mathbf{0}$. Letting $\mathbf{f}$ denote the resultant thrust force per unit mass of B, and letting $\hat{\mathbf{n}}_1$, $\hat{\mathbf{n}}_2$, and $\hat{\mathbf{n}}_3$ be three mutually perpendicular unit vectors fixed in N, one can obtain an accurate assessment of the issue by calculating three velocity increments as $\Delta V_r = \int \mathbf{f} \cdot \hat{\mathbf{n}}_r\, dt$ $(r = 1, 2, 3)$. In the present example, the total velocity increment is found to be 0.0073 m/s; using an initial mass of $m_0 = (1.118 \times 10^6 - 108)$ kg together with the rocket equation, one can determine the corresponding mass of SEP propellant to be $\Delta m = 0.2785$ kg. Thus, in this case, the failure to apply thrust as a couple is hardly detrimental. More generally, an upper bound on Δm can be estimated by assuming $\mathbf{f}$ is constant in N for, say, 1800 s (30 min), with $\mathbf{f} = [(400\,\hat{\mathbf{n}}_1 + 400\,\hat{\mathbf{n}}_2)/1.118 \times 10^6]$ m/s^2. Using the resultant of $\mathbf{f}$, one obtains $\Delta V = \sqrt{2}(3.5778 \times 10^{-4}$ m/s$^2)(1800$ s$) = 0.91$ m/s, and a corresponding mass of SEP propellant $\Delta m = 34.6$ kg. In the worst case, then, the net savings in propellant mass is still almost 150 kg.

7. Conclusions

Changing the trajectory and rotational motion of an asteroid, whether for the purpose of retrieving it, deflecting it, or using it to deflect a larger asteroid, will likely involve some or all of the spacecraft motions considered here: approaching, hovering, synchronizing the rotational motion of the spacecraft with the asteroid, descending, ascending, and arresting the angular velocity of the asteroid. A preliminary study of the dynamics and control of these motions has been conducted in order to understand the magnitude of the required velocity increments, attitude control torque, and the associated propellant mass for a particular spacecraft and reaction control system.

Gravitational forces exerted by the asteroid on the spacecraft are neglected. (Although this is justified in the case of a 10-m asteroid, it becomes less justified as asteroid mass increases.) Initial approach, hovering, descent, and ascent are examined for asteroids performing what is essentially simple rotational motion at angular speeds of 0.5, 1, 5, 10, and 60 revolutions per hour. The axis of rotation is essentially in the plane of the asteroid's heliocentric orbit, and perpendicular to local vertical. Initial approaches that end in conditions suitable for hovering appear to be relatively inexpensive when using minimum-ΔV, multi-impulse trajectories. Closed-form expressions are presented for ΔV required to hover for one revolution. Hovering over one of the poles costs nothing; however, the cost escalates as the latitude approaches the equator, and

as the angular speed increases, and can become prohibitive. (Gravitational attraction may reduce the cost somewhat in the case of a large, slowly rotating asteroid.) As for descent and ascent, expense again increases in connection with equatorial regions and high angular speeds. Time of flight also enters the picture, and in some cases cost can be minimized with respect to time of flight.

Two attitude control algorithms have been developed, and both are demonstrated with examples involving tumbling rotational motion of an unsymmetric rigid body. In the first case, the controller is used to synchronize angular velocity of the spacecraft with that of the asteroid, while the spacecraft's axis of symmetry is kept parallel to a line fixed in the asteroid. The amount of propellant required is moderate, despite the asteroid's high angular speeds. In the second case, an asymptotically stable controller arrests the angular velocity of an asteroid that is rigidly attached to the spacecraft. Rotational kinetic energy can be dissipated slowly or quickly, depending on the premium one places on control effort. A novel approach is applied to an example involving what is at first simple rotation: a perturbation induces tumbling, and this allows the use of long thrust moment arms that otherwise would not come into play. Propellant consumption is reduced by a factor of three, compared to an arrest in which simple rotational motion is maintained.

In future work, we intend to improve the aforementioned analyses by accounting for gravitational attraction of the asteroid. Solar arrays needed for the solar electric propulsion system will be large, and therefore solar radiation pressure will also be modeled. Treatment of the reaction control system will be refined by considering minimum firing times and minimum thrust levels.

References

[1] Brophy, J., et al., "Asteroid Retrieval Feasibility Study," Keck Institute for Space Studies, Pasadena, California, April 2, 2012. http://kiss.caltech.edu/study/asteroid/asteroid_final_report.pdf (Accessed January 23, 2013.)

[2] Dunham, D., et al., "Deflecting Hazardous Asteroids from Collision with the Earth by using Small Asteroids," IAA-PDC13-04-16P, 2013 Planetary Defense Conference, April 15–19, 2013.

[3] Kaplan, M. H., *Modern Spacecraft Dynamics and Control*, Wiley, New York, 1976.

[4] Kane, T. R., Likins, P. W., and Levinson, D. A., *Spacecraft Dynamics*, McGraw-Hill, New York, 1983.

[5] Tsiotras, P., and Longuski, J. M., "Spin-Axis Stabilization of Symmetric Spacecraft with Two Control Torques," *Systems and Control Letters*, Vol. 23, No. 6, 1994, pp. 395–402.

[6] Slotine, J.-J. E., and Li, W., *Applied Nonlinear Control*, Prentice-Hall, Inc., Englewood Cliffs, NJ, 1991.